Journal of Computational Physics **178,** 290–306 (2002)
doi:10.1006/jcph.2002.7014, available online at http://www.idealibrary.com on IDEAL®

High-Order Time-Stable Numerical Boundary Scheme for the Temporally Dependent Maxwell Equations in Two Dimensions

J. F. Nystrom[1]

MRC Institute, Moscow, Idaho 83844-1024
E-mail: nystrom@sci.tamucc.edu

Received September 17, 1999; revised March 7, 2001

High-order time-stable boundary operators for perfectly electrically conducting (PEC) surfaces are presented for a 3×3 hyperbolic system representing electromagnetic fields TE to z. First a set of operators satisfying the summation-by-parts property are presented for a 2×2 hyperbolic system representing one-dimensional electromagnetic propagation in a PEC cavity. Boundary operators are then developed for two-dimensional electromagnetic propagation in the xy-plane. This procedure leads to a time-stable scheme for a 3×3 hyperbolic system and concurrently shows how to eliminate the ambiguity associated with tangential and normal electromagnetic field components at corners and edges of PEC scatterers when using colocated computational electromagnetic schemes. A numerical comparison to the popular Yee scheme is included, and this comparison suggests that the fourth-order (in space and time) scheme derived herein does effectively compute the Maxwell equations in two dimensions.

Key Words: stability and convergence of difference methods; electromagnetics.

1. INTRODUCTION

In computational electromagnetics (CEM) simulations, the desire to model electrically large objects creates a need for high-order algorithms. Furthermore, to achieve pth-order of spatial accuracy in a computation, it is well-known that the boundary must be closed with at least a $(p-1)$th-order operator [1]. Herein, we refer to boundary operators of accuracy ≥ 3 as high-order boundary operators, and in CEM the implementation of high-order boundary operators near perfectly electrically conducting (PEC) boundaries is currently very problematical [2]. When encountering boundaries, most high-order CEM schemes will use a transition zone of stencils between the high-order interior stencil and the lower

[1] Current address: Texas A&M University, Corpus Christi, Texas 78412.

0021-9991/02 $35.00

order boundary stencil. In this investigation, the time stability [1] and spatial stencils for high-order boundary operators are developed concurrently. To create the time-stable fourth-order (in space and time) algorithm presented herein, a standard fourth-order Runge–Kutta (RK4) integrator is used to advance the equations in time, while the spatial stencils and boundary operator methodology is based on *summation-by-parts* [3–9] techniques. Parenthetically, if u represents a solution vector, then for a continuous u, we let Lu represent $\partial u/\partial x$. (We are interested in accurate and stable finite difference approximations of Lu.) For the semidiscretization of the continuous derivative, let H be the norm matrix, let $\bar{u}$, $\bar{v}$ be the discrete grid vectors (where, e.g., $\bar{u} = (u_0 u_1 \cdots u_N)^T$) approximating u and v, and let Q be the difference matrix. For a closed domain, a difference operator having the summation-by-parts property must satisfy the norm

$$\begin{aligned}(\bar{u}, Q\bar{u}) &= \langle \bar{u}, HQ\bar{u} \rangle \\ &= -\frac{1}{2}u_0^2 + \frac{1}{2}u_N^2,\end{aligned} \tag{1}$$

where H is the *specific* norm matrix associated with the difference matrix Q. Evidently for an operator Q which satisfies the summation-by-parts rule, the norm depends only on the boundary data. To show stability for hyperbolic first-order systems, restricted full norms or diagonal norms must be used, and to show stability for systems in several space dimensions, diagonal norms are required [3, 6, 8]. Herein, we show results with restricted full norm and diagonal norm operators in one dimension and utilize only a diagonal norm for the two-dimensional developments.

In this paper a time-stable fully fourth-order explicit treatment of electromagnetic fields TE to z (TE_z) is derived. In Section 1 the case of one-dimensional electromagnetic (EM) propagation is cast in the form of a 2×2 hyperbolic system. The complete initial boundary value problem (IBVP), written in a form capable of handling both the total field and scattered field formulations, is presented, and the orthogonal projection method of Olsson [3, 4] is introduced as a technique for handling the boundary conditions of the field components at PEC walls. Various spatial stencils which satisfy a summation-by-parts formula are shown to effectively track the time development of an EM pulse in a PEC cavity. In Section 2 the techniques utilized in Section 1 are expanded to include a treatment for corners in a two-dimensional computational domain. Projection operators are developed and a fully discrete version of the 3×3 hyperbolic system describing TE_z mode propagation is presented. Numerical comparison to the popular CEM method, the Yee scheme, is provided in Section 2. In general, many comments specific to the CEM implementation are included, but an emphasis is placed on presenting the problem of electromagnetic wave propagation as an important case study for the theories and techniques advocated herein.

2. ONE-DIMENSIONAL EM WAVE PROPAGATION

For one-dimensional propagation in the z-direction, the Maxwell curl equations [10] reduce to

$$\begin{aligned}\frac{\partial E_x}{\partial t} &= -c^2 \frac{\partial B_y}{\partial z}, \\ \frac{\partial B_y}{\partial t} &= -\frac{\partial E_x}{\partial z}.\end{aligned} \tag{2}$$

Let

$$w = \begin{bmatrix} E_x \\ cB_y \end{bmatrix}; \tag{3}$$

then Eq. (2) can then be written as a 2×2 hyperbolic system,

$$w_t = A\, w_z, \tag{4}$$

where

$$w_t = \frac{\partial}{\partial t} \begin{bmatrix} E_x \\ cB_y \end{bmatrix}, \quad w_z = \frac{\partial}{\partial z} \begin{bmatrix} E_x \\ cB_y \end{bmatrix}, \tag{5}$$

and

$$A = \begin{bmatrix} 0 & -c \\ -c & 0 \end{bmatrix}. \tag{6}$$

In CEM the matrix A is commonly called a *connectivity* matrix.

For notational purposes, let $B_y \to B$ and $E_x \to E$; then the grid vector for the spatially discrete system is written as

$$\bar{w} = (E_0\, cB_0\, E_1\, cB_1 \ldots E_N\, cB_N)^T. \tag{7}$$

We desire the semidiscrete equation

$$\frac{d\bar{w}}{dt} = \bar{M}\bar{w}, \tag{8}$$

where according to our program $\bar{M}$ must satisfy the summation-by-parts formula (e.g., Eq. (1)). When moving from the continuous representation of the one-dimensional system, Eq. (4), to the semidiscretization of the system, Eq. (8), it is required that Eq. (6) be modified such that

$$\bar{A} = \begin{bmatrix} 0 & -c & & & 0 \\ -c & 0 & & & \\ & & 0 & -c & \\ & & -c & 0 & \\ & & & & \ddots \\ 0 & & & & \end{bmatrix}. \tag{9}$$

Let Q be a difference operator approximating $\partial/\partial z$. For reasons outlined in the Introduction, we restrict our attention in this section to two operators which satisfy the summation-by-parts formula: the RF4, a restricted full norm operator, and the D4, a diagonal norm operator.

Specifically, the RF4 operator (for the scalar case) has the form

$$hQ = \begin{bmatrix} \frac{-11}{6} & 3 & \frac{-3}{2} & \frac{1}{3} & 0 & 0 & 0 & 0 & 0 & 0 & \cdots \\ q_{10} & q_{11} & q_{12} & q_{13} & q_{14} & q_{15} & q_{16} & 0 & 0 & 0 & \\ q_{20} & q_{21} & q_{22} & q_{23} & q_{24} & q_{25} & q_{26} & 0 & 0 & 0 & \\ q_{30} & q_{31} & q_{32} & q_{33} & q_{34} & q_{35} & q_{36} & 0 & 0 & 0 & \\ q_{40} & q_{41} & q_{42} & q_{43} & q_{44} & q_{45} & q_{46} & 0 & 0 & 0 & \\ 0 & 0 & 0 & \frac{1}{12} & \frac{-2}{3} & 0 & \frac{2}{3} & \frac{-1}{12} & 0 & 0 & \\ 0 & 0 & 0 & 0 & \frac{1}{12} & \frac{-2}{3} & 0 & \frac{2}{3} & \frac{-1}{12} & 0 & \\ \vdots & & & & & & & & & \ddots & \end{bmatrix}, \tag{10}$$

where the coefficients q_{ij} are given in an appendix of [6]. The coefficients in Eq. (10) encompass the transition zone between a third-order windward stencil on the boundary and a fourth-order central operator in the interior. Furthermore, these coefficients are designed so that the semidiscretization satisfies a summation-by-parts energy norm [6, 9]. The specific D4 stencil used herein is the minimum bandwidth fourth-order diagonal norm difference operator [6], which is shown in Eq. (11) (again for a scalar case):

$$hQ = \begin{bmatrix} q_{00} & q_{01} & q_{02} & q_{03} & q_{04} & 0 & 0 & 0 & 0 & 0 & 0 & \cdots \\ q_{10} & 0 & q_{12} & q_{13} & q_{14} & q_{15} & 0 & 0 & 0 & 0 & 0 & \\ q_{20} & q_{21} & 0 & q_{23} & q_{24} & q_{25} & 0 & 0 & 0 & 0 & 0 & \\ q_{30} & q_{31} & q_{32} & 0 & q_{34} & q_{35} & q_{36} & 0 & 0 & 0 & 0 & \\ q_{40} & q_{41} & q_{42} & q_{43} & 0 & q_{45} & q_{46} & q_{47} & 0 & 0 & 0 & \\ 0 & q_{51} & q_{52} & q_{53} & q_{54} & 0 & q_{56} & q_{57} & q_{58} & 0 & 0 & \\ 0 & 0 & 0 & \frac{-1}{60} & \frac{3}{20} & \frac{-3}{4} & 0 & \frac{3}{4} & \frac{-3}{20} & \frac{1}{60} & 0 & \\ 0 & 0 & 0 & 0 & \frac{-1}{60} & \frac{3}{20} & \frac{-3}{4} & 0 & \frac{3}{4} & \frac{-3}{20} & \frac{1}{60} & \\ \vdots & & & & & & & & & & & \ddots \end{bmatrix} \tag{11}$$

As was done for the A matrix in Eq. (9), when converting from the scalar case to the discrete system case, the Q matrix and norm matrix H, say, for the D4 operator, take on the form

$$h\bar{Q} = \begin{bmatrix} q_{00} & 0 & q_{01} & \cdots \\ 0 & q_{00} & 0 & \\ \vdots & & & \ddots \end{bmatrix} \tag{12}$$

and

$$\bar{H} = \begin{bmatrix} h_{00} & 0 & 0 & \cdots \\ 0 & h_{00} & 0 & \\ 0 & 0 & h_{11} & \\ \vdots & & & \ddots \end{bmatrix}. \tag{13}$$

For the semidiscrete equation, Eq. (8), it was found (using *Mathematica* [11] on a twenty-cell

domain) that both an RF4 and a D4 stencil-based scheme give the norm (with $\bar{M} = \bar{A}\bar{Q}$)

$$\begin{aligned}(\bar{w}, \bar{M}\bar{w}) &= \langle \bar{w}, \bar{H}\bar{A}\bar{Q}\bar{w} \rangle \\ &= -\frac{1}{2}\bar{w}_0^2 - \frac{1}{2}\bar{w}_1^2 + \frac{1}{2}\bar{w}_{2N-1}^2 + \frac{1}{2}\bar{w}_{2N}^2 \\ &= -\frac{1}{2}E_0^2 - \frac{1}{2}(cB_0)^2 + \frac{1}{2}E_N^2 + \frac{1}{2}(cB_N)^2,\end{aligned}$$

which shows that the norm only depends on the boundary data (cf. Eq. (1)).

Following [7, 8], the system in Eq. (4) is now modified to model closely a scattered field formulation (e.g., for the scattered field formulation we input values for the scattered tangential electric fields on PEC boundaries, while in a total field formulation we set $E_{\tan}$ on all PEC boundaries to zero). For a PEC cavity with walls at $z = 0$ and $z = 1$, the inhomogeneous IBVP is written as

$$\begin{aligned} w_t &= Aw_z, \quad 0 \le z \le 1, t \ge 0, \\ w(z, 0) &= f(z), \quad 0 \le z \le 1, \\ w(0, t) &= g(t), \quad t \ge 0, \\ w(1, t) &= h(t), \quad t \ge 0. \end{aligned} \tag{14}$$

For the scattered field formulation, we impose the negative values of the incident tangential electric fields at PEC boundaries, which, with $g^T = [g_{E_0} 0]$, corresponds to letting

$$g_{E_0}(t) = -E^{\text{inc}}(0, t).$$

For the discrete system, the boundary condition at $z = 0$ is couched in terms of a boundary operator L as

$$L^T \bar{w} = g_{E_0}, \quad L^T = [1 \quad 0 \quad \cdots \quad 0]. \tag{15}$$

By construction, the orthogonal projection operator [3, 4, 8] is designed to provide a stable method of introducing the analytical boundary conditions. Given the boundary operator L, the projection operator P for restricted full or diagonal norms is given as

$$P = I - L(L^T L)^{-1} L^T. \tag{16}$$

This projection operator will modify the semidiscrete equation, Eq. (8), such that for homogeneous boundary conditions (i.e., $g = h = 0$ in Eq. (14)), we can write

$$\frac{d\bar{w}}{dt} = P\bar{M}\bar{w}. \tag{17}$$

For the semidiscrete scattered field formulation of Eq. (14), let

$$\tilde{\mathrm{g}} = \begin{bmatrix} -E^{\text{inc}}(0, t) \\ 0 \\ \vdots \\ 0 \\ -E^{\text{inc}}(1, t) \\ 0 \end{bmatrix}, \tag{18}$$

and

$$L^T = \begin{bmatrix} 1 & 0 & \cdots & 0 & 0 & 0 \\ 0 & 0 & \cdots & 0 & 1 & 0 \end{bmatrix}. \tag{19}$$

The projection operator is obtained by using Eq. (19) in Eq. (16), and the theory gives the final version of the semidiscretization of the IBVP in Eq. (14) as

$$\bar{w}_t = P\bar{M}\bar{w} + (I - P)\tilde{g}_t. \tag{20}$$

The solution vector, $\bar{w}$, is obtained by integrating Eq. (20) at all points using the RK4 integrator. Note that in Eq. (20) the boundary condition is imposed in terms of its time derivative. If the time derivative of the analytical boundary condition is unavailable, we can use an auxiliary variable as shown in [7] to couch the problem solely in terms of $\tilde{g}$, rather than $\tilde{g}_t$.

2.1. One-Dimensional PEC Cavity

In this section, we discuss a measure of the spatial operator accuracy, and also show time developments of EM pulses in a PEC cavity. These one-dimensional tests utilize the RK4 integrator in conjunction with the RF4 and D4 difference stencils. The PEC cavity tests model Eq. (2); thus propagation is in the $\pm z$-direction.

To validate experimentally the order of accuracy of the RF4 and D4 operators, the following test is considered. Let $u = \sin(kx)$ with $k = 2\pi$. Let ε be the $\mathcal{L}_2$ norm of the error between the computed value and the exact value, and let h be the grid spacing. In accordance with Taylor theory, $\log(\varepsilon)/\log(h)$ is proportional to the order of the scheme, for a reasonably small h. Such is the case for both the RF4 and D4 operators, as borne out in Fig. 1.

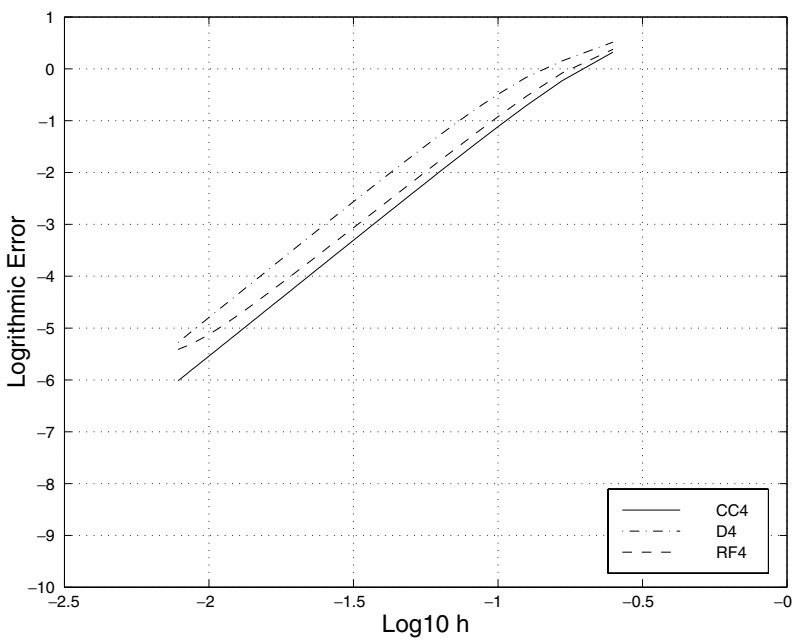

FIG. 1. Grid refinement for the RF4, D4, and CC4 spatial operators.

The CC4 stencil, also included in Fig. 1, is a high-order spatially implicit stencil. Details of the CC4–RK4 scheme are discussed in [12]. The error is calculated over the whole domain and includes the boundaries.

In all time-domain simulations, the fields are modeled using a Gaussian pulse of the form $e^{-a^2\tau^2}$, where a controls the pulse width and $\tau = (v_p(t - t_0) + (x - x_0))$. The pulse bandwidth is defined to be from zero to ω_m (or from 0 to f_m, where $\omega_m = 2\pi f_m$), where ω_m is the angular frequency for which the frequency-domain amplitude of the pulse is one-tenth of its peak value. The correlation between a and ω_m is deduced from Fourier analysis: $a = \omega_m/(3.035c)$. Furthermore, let $\lambda_{min} = 2\pi/k_{max}$ with $k_{max} = \omega_m/c$. We choose to set h using λ_{min}/N_{pts}, where N_{pts} is the number of points per wavelength associated with ω_m. Unless otherwise noted $v_p = 1$ m/s, $f_m = 2$ GHz, and $c = 3E^8$ m/s. The time step in one dimension is related to the special step size as $dt = (CFL\ \ h)/v_p$.

One-dimensional tests of these high-order schemes using the RK4 integrator in conjunction with the RF4 and D4 difference stencils in the PEC cavity were performed in both the total field and the scattered field formulations, with and without a dielectric slab in the cavity. For the D4 examples we use the scattered field formulation, with an EM pulse as input. Therefore, for the D4 runs, the governing equation is given by Eq. (20), with $f(z)$ in Eq. (14) set to zero over the entire domain. Figure 2 shows the time development for the pulse over a long range of time steps, with a $CFL = 1$. Figure 3 shows a late time run after the pulse has traveled 100,000 cells, using a $CFL = 1.78$. The RF4 tests used the total field formulation. For these total field tests, an EM pulse is setup at $t = 0$ using $f(z)$ and setting $g = h = 0$ in Eq. (14), effectively giving Eq. (14) as the governing equation. Figure 4 shows the time development for the pulse over a long range of time steps, using a

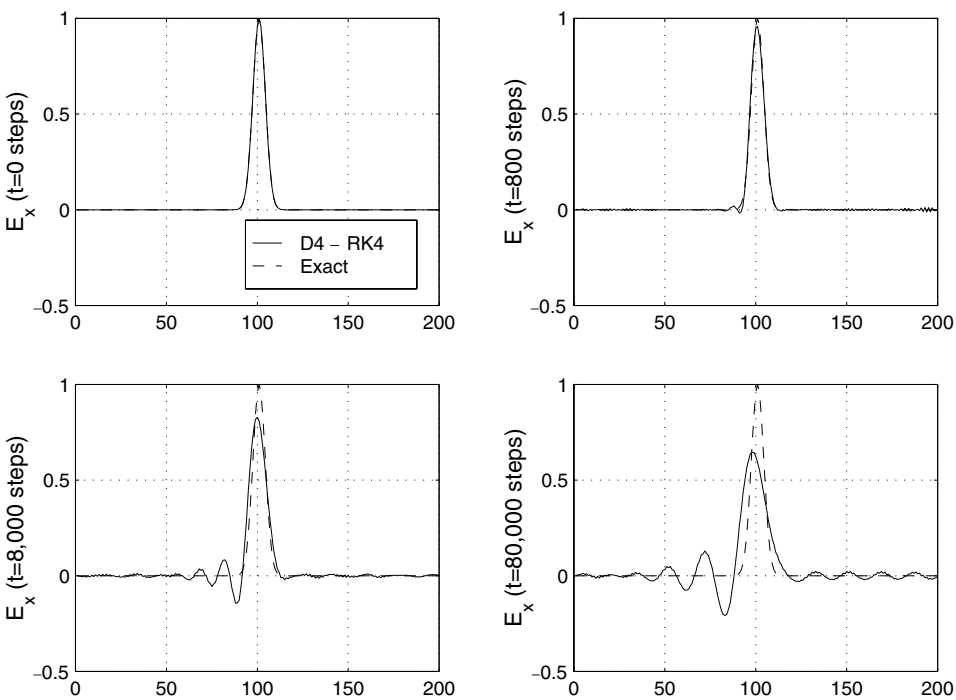

FIG. 2. Time development for the D4–RK4 scheme, CFL = 1.

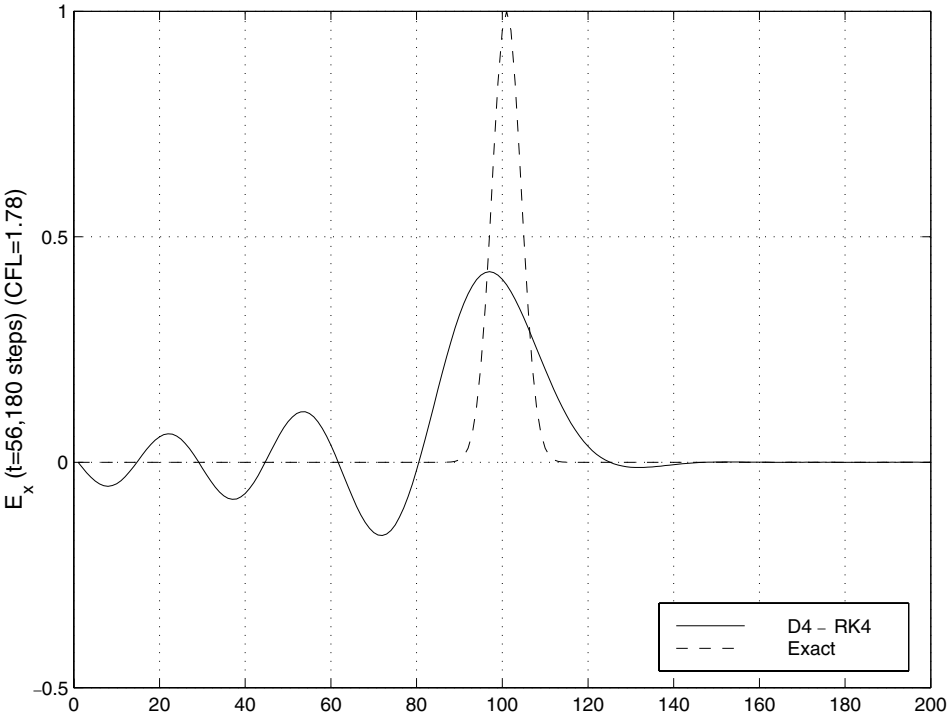

FIG. 3. Late time data for the D4–RK4 scheme, CFL = 1.78.

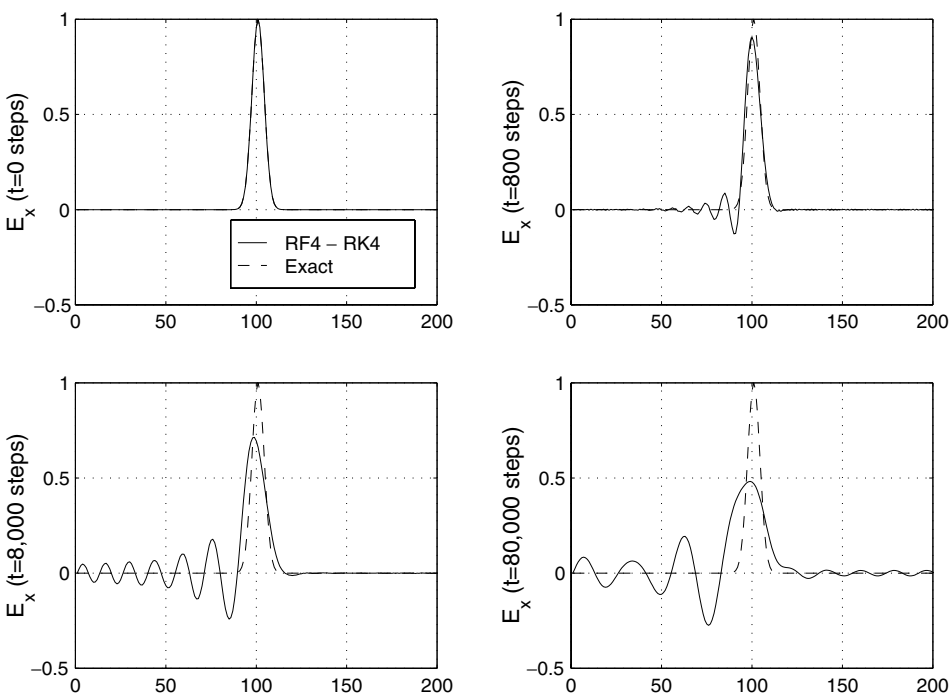

FIG. 4. Time development for the RF4–RK4 scheme, CFL = 1.

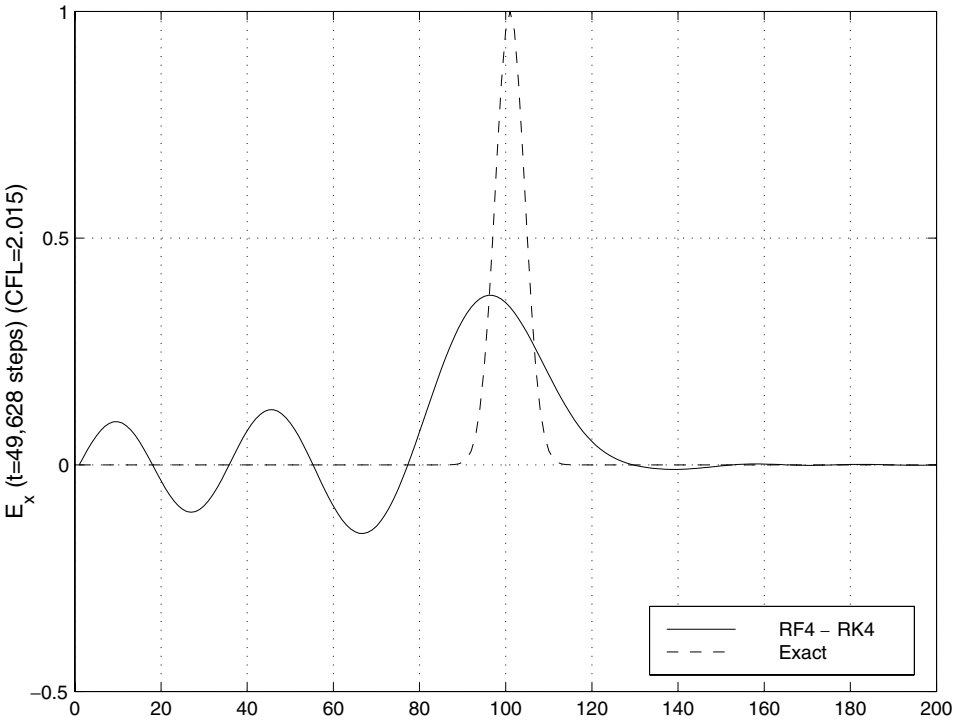

FIG. 5. Late time data for the RF4–RK4 scheme, CFL = 2.015.

$CFL = 1$. Figure 5 shows a late time run after the pulse has traveled 100,000 cells, using a $CFL = 2.015$.

3. TWO-DIMENSIONAL EM WAVE PROPAGATION

In order to extend the techniques for one-dimensional propagation to the case of two-dimensional propagation, we are required to reformulate the projection operator in terms of the characteristic variables of the system. Here we follow [3] in the development of a projection operator that handles corners for two-dimensional PEC scatterers.

For TE_z mode propagation in the xy-plane, the Maxwell curl equations reduce [10] to

$$\begin{aligned} \frac{\partial E_x}{\partial t} &= c^2 \frac{\partial B_z}{\partial y}, \\ \frac{\partial E_y}{\partial t} &= -c^2 \frac{\partial B_z}{\partial x}, \\ \frac{\partial B_z}{\partial t} &= \left(\frac{\partial E_x}{\partial y} - \frac{\partial E_y}{\partial x} \right). \end{aligned} \tag{21}$$

The solution vector, u, is given as

$$u = \begin{bmatrix} E_x \\ E_y \\ cB_z \end{bmatrix}. \tag{22}$$

Equation (21) can now be written as a 3×3 hyperbolic system,

$$u_t = P_x\, u_x + P_y\, u_y, \tag{23}$$

where

$$u_t = \frac{\partial}{\partial t}\begin{bmatrix} E_x \\ E_y \\ cB_z \end{bmatrix}, \quad u_x = \frac{\partial}{\partial x}\begin{bmatrix} E_x \\ E_y \\ cB_z \end{bmatrix}, \quad u_y = \frac{\partial}{\partial y}\begin{bmatrix} E_x \\ E_y \\ cB_z \end{bmatrix}, \tag{24}$$

and

$$P_x = \begin{bmatrix} 0 & 0 & 0 \\ 0 & 0 & -c \\ 0 & -c & 0 \end{bmatrix}, \quad P_y = \begin{bmatrix} 0 & 0 & c \\ 0 & 0 & 0 \\ c & 0 & 0 \end{bmatrix}. \tag{25}$$

For notational purposes let $E_x \to E^x$ and $E_y \to E^y$. The grid vector u is written [4] as $u^T = (u_0^T \ \ldots \ u_N^T)$ with $u_j^T = (u_{0j}^T \ \ldots \ u_{Mj}^T)$ such that $u_{ij} \in R^d$, for a domain with limits of $i \in 0, \ldots, M$ and $j \in 0, \ldots, N$. For this two-dimensional hyperbolic system, $d = 3$, and the grid vector for u has $d \times (M+1) \times (N+1)$ elements and is written as

$$\bar{u}^T = \left(E_{00}^x\, E_{00}^y\, cB_{00}\, E_{10}^x \ \ldots \ cB_{(M-1)N}\, E_{MN}^x\, E_{MN}^y\, cB_{MN}\right). \tag{26}$$

Here in Eq. (26), we have $\bar{u}_0^T = (E_{00}^x\, E_{00}^y \ \ldots \ cB_{M0})$, where $\bar{u}_{00}^T = (E_{00}^x\, E_{00}^y\, cB_{00}) \in R^3$. That is, $\bar{u}_{00}$ is a three-element column vector.

For this TE_z mode, we find that on a boundary surface that lies along a coordinate axis, one component of the **E**-field will be normal to the surface, while the other component will be tangential. The physical boundary condition on the PEC surface [10] for the electric field dictates that the normal component be proportional to the surface charge, while the total (i.e., incident plus scattered) tangential component should vanish. Furthermore, for the fully discrete case, we find that on each boundary surface that lies along a coordinate axis, the derivatives normal to the surface maintain a one-dimensional character [3, 13], while the derivatives tangential to the surface will be treated in a special manner. For derivatives tangential to a surface, we treat the surface as a closed one-dimensional domain, requiring boundary closure at each extremum of the surface. When two separate planar surfaces meet, a corner node is established at the intersection point. While the interior of each planar surface is handled as previously described, the time evolution of the field components at the corner node are given special treatment. For the corners of a PEC scatterer we require a method to determine which field components are tangential, and which components are normal at said corner. For the system shown in Eq. (23), in order to formulate the governing equations for the dependent variable at a corner, we need to specify the relationship between the ingoing and outgoing characteristics at the corner.

To establish this relationship (between the ingoing and outgoing characteristics) we present the following derivation. Let $n = (n_x, n_y)$ be the outward unit normal to the surface (which is to be constructed). This normal is defined such that $h = \sqrt{h_x^2 + h_y^2}$ and

$$n_x = \frac{-h_y}{h}, \quad n_y = \frac{-h_x}{h}\,. \tag{27}$$

Note that a definitive normal can be established for all points on the boundary. At each point on a boundary a matrix A is formed,

$$A = n_x P_x + n_y P_y, \tag{28}$$

where P_x and P_y are given in Eq. (25). The matrix A can be diagonalized anywhere on the surface, giving (with Q representing the modal matrix [14])

$$\Lambda = Q^T A Q, \tag{29}$$

whose diagonal elements are the eigenvalues of A. As with all similarity transformations [14], the matrix Q is built up with the eigenvectors of A.

After the construction of A and the calculation of the modal matrix Q, the following observations are in order. The characteristic variables on the boundary are given by $\varphi = Q^T u$. We can split the characteristics (i.e., the elements of φ) into separate vectors representing the ingoing and outgoing characteristics. Specifically, let φ_I be the ingoing characteristics and let φ_{II} represent the outgoing characteristic variables. For a solution vector $u \in R^d$, we require that $\varphi_I \in R^{d_1}$ and $\varphi_{II} \in R^{d_2}$ such that $d_1 + d_2 = d$. For example, with $d = 3$, we may have $d_1 = 1$ and $d_2 = 2$. We desire to build a relationship between φ_I and φ_{II}. This relationship (between φ_I and φ_{II}) is written as

$$\varphi_I = S \varphi_{II}, \tag{30}$$

which yields values for the (newly defined) matrix S. Furthermore, after we define Q_I and Q_{II} such that $\varphi_I = Q_I^T u$ and $\varphi_{II} = Q_{II}^T u$, then a boundary operator L can be constructed.

$$L^T u = 0 \tag{31}$$

such that

$$L^T = Q_I^T - S Q_{II}^T, \tag{32}$$

where the S matrix is governed by Eq. (30). The boundary operator L can in many cases be written down by inspection of what is dictated by the result in Eq. (31) for any one specific boundary condition.

As an example of the methodology, we use the theory to construct a boundary operator at a corner. For a domain with boundaries along the x-axis and y-axis, the origin, $(0, 0)$, serves as a corner to the domain. At the origin, we use Eq. (32) to calculate the boundary operator L. We denote the connectivity matrix at this corner as A_{00}. The matrix A_{00}, at a corner with a normal by $n_x = n_y = -1/\sqrt{2}$, is calculated using Eq. (28):

$$A_{00} = \frac{1}{\sqrt{2}} \begin{bmatrix} 0 & 0 & -c \\ 0 & 0 & c \\ -c & c & 0 \end{bmatrix}. \tag{33}$$

During the construction of the eigenvalue matrix at this corner, $\Lambda_{00} = \text{diag}\{\mp c, 0\} =$

$Q^T\, A_{00}\, Q$, the eigenvector matrix Q is found to be

$$Q = \frac{1}{\sqrt{2}} \begin{bmatrix} 1/\sqrt{2} & -1/\sqrt{2} & 1 \\ -1/\sqrt{2} & 1/\sqrt{2} & 1 \\ 1 & 1 & 0 \end{bmatrix}. \tag{34}$$

Accordingly, the characteristic variables are given as $\varphi = Q^T u$, yielding

$$\varphi = \frac{1}{\sqrt{2}} \begin{bmatrix} E_x/\sqrt{2} - E_y/\sqrt{2} + cB_z \\ -E_x/\sqrt{2} + E_y/\sqrt{2} + cB_z \\ E_x + E_y \end{bmatrix}. \tag{35}$$

Attention is now focused on the ingoing and outgoing characteristics for TE_z modes. For this particular PEC corner, given $E_{\tan} = 0$, we require that $E_x = E_y$, which yields the following characteristics:

$$\varphi_I = \frac{1}{\sqrt{2}}[cB_z] \tag{36}$$

and

$$\varphi_{II} = \frac{1}{\sqrt{2}} \begin{bmatrix} cB_z \\ E_x + E_y \end{bmatrix}. \tag{37}$$

We use Eq. (36) and Eq. (37) in Eq. (30) to obtain $S = [1 \quad 0]$ at this corner. From Eq. (32), it follows that

$$L^T = [-1 \quad 1 \quad 0], \tag{38}$$

which specifies that $E_x = E_y$ at this corner (i.e., $L^T u = 0$). We now use Eq. (38) in Eq. (16) to obtain the projection operator:

$$P = \begin{bmatrix} 1/2 & 1/2 & 0 \\ 1/2 & 1/2 & 0 \\ 0 & 0 & 1 \end{bmatrix}. \tag{39}$$

For the TE_z scattered field formulation we modify Eq. (23) as done in Eq. (20) [3].

$$u_t = PP_x u_x + PP_y u_y + (I - P)\tilde{\mathrm{g}}_t, \tag{40}$$

where $\tilde{\mathrm{g}}$ incorporates the boundary condition as shown in Eq. (18), and $\tilde{\mathrm{g}}_t$ is the time derivative of $\tilde{\mathrm{g}}$. We expand Eq. (40) for the TE_z case to obtain the linear system

$$\begin{bmatrix} \dfrac{\partial E_x}{\partial t} \\ \dfrac{\partial E_y}{\partial t} \\ c\dfrac{\partial B_z}{\partial t} \end{bmatrix} = \begin{bmatrix} -\dfrac{c^2}{2}\dfrac{\partial B_z}{\partial x} \\ -\dfrac{c^2}{2}\dfrac{\partial B_z}{\partial x} \\ -c\dfrac{\partial E_y}{\partial x} \end{bmatrix} + \begin{bmatrix} \dfrac{c^2}{2}\dfrac{\partial B_z}{\partial y} \\ \dfrac{c^2}{2}\dfrac{\partial B_z}{\partial y} \\ c\dfrac{\partial E_x}{\partial y} \end{bmatrix} + \begin{bmatrix} -\dfrac{1}{2}\dfrac{\partial}{\partial t}\left(E_x^{\mathrm{inc}} - E_y^{\mathrm{inc}}\right) \\ -\dfrac{1}{2}\dfrac{\partial}{\partial t}\left(E_y^{\mathrm{inc}} - E_x^{\mathrm{inc}}\right) \\ 0 \end{bmatrix}, \tag{41}$$

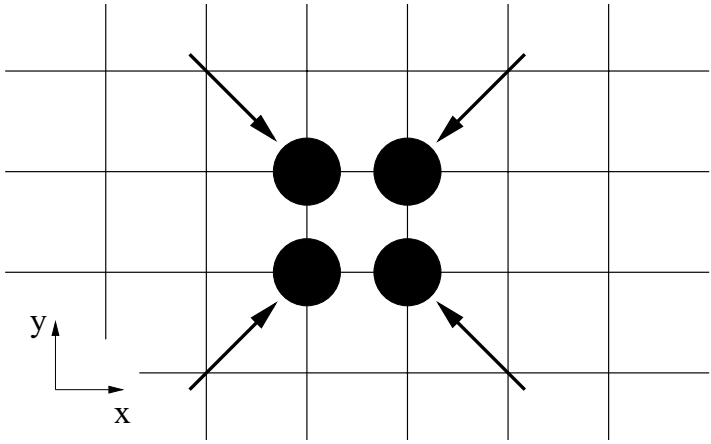

FIG. 6. Line source with outward normal at each node on the boundary.

which is valid only *at* a specific corner of a PEC scatterer with an inward normal (to the surface) given by $n = (\pm 1/\sqrt{2}, \pm 1/\sqrt{2})$.

As seen in Fig. 6, for a simple shape like a line source, a square, or rectangular cylinder, there need be only two distinct types of corner nodes. To make clear what the linear system in Eq. (41) dictates, consider the following. When we implement a semidiscrete approximation of Eq. (41), i.e., when, say, the D4 operator is used to approximate the continuous partial derivative $\partial/\partial x$, we find that the time evolution of E_x and E_y at this corner no longer depends solely on a single spatial derivative of B_z (as shown in Eq. (21)). Rather, when using Eq. (41) to evolve the field components at this corner, the cells used to update E_x and E_y are located at the corner and *off* the plate for convex corners, forming a stencil footprint in the shape of an "L," whose corner is located at the boundary cell. That is, E_x and E_y each depend on spatial derivatives in both the x- and y-directions. This system will maintain $E_{\text{tan}} = 0$ (as a matter of course in the total field formulation, and also in the scattered field formulation when the incident field is added in). Furthermore, E_{normal} to the boundary evolves according to the change of B_z in both the x- and y-directions.

It is important to realize at this point that there is no longer any question which vector field components are normal and which are tangential at a corner of a PEC scatterer (or any other type of object). This is a result of effectively chamfering the corner, and establishing a definite normal for the object at the corner. Parenthetically, it should be easy to show that a surface normal of arbitrary orientation can be included in a computational domain using the techniques described herein. As an example we derive the linear system describing the time evolution of the fields at a PEC corner whose surface tangent makes a 60° angle with the x-axis. For this surface, the surface normal is given as $n = (\sqrt{3}/2, 1/2)$, and it then follows that

$$A = \frac{1}{2}\begin{bmatrix} 0 & 0 & c \\ 0 & 0 & -\sqrt{3}c \\ c & -\sqrt{3}c & 0 \end{bmatrix}.$$

At this location, $E_{\text{tan}} = 0$ dictates that $E_x = \sqrt{3}E_y$, which yields the characteristics

$$\varphi_I = \frac{1}{\sqrt{2}}[cB_z]$$

and

$$\varphi_{II} = \frac{1}{\sqrt{2}} \begin{bmatrix} 2\sqrt{2}E_y \\ cB_z \end{bmatrix}.$$

Formulating $\varphi_I = S\varphi_{II}$ yields $S = [0\ \ 1]$, and it follows that

$$L^T = Q_I^T - SQ_{II}^T = \frac{1}{\sqrt{2}}[1 \quad -\sqrt{3} \quad 0].$$

Upon calculation of the projection operator we obtain the linear system describing the time evolution of the field components at this specific type of corner (shown here in the total-field formulation):

$$\begin{bmatrix} \dfrac{\partial E_x}{\partial t} \\ \dfrac{\partial E_y}{\partial t} \\ c\dfrac{\partial B_z}{\partial t} \end{bmatrix} = \begin{bmatrix} -\dfrac{\sqrt{3}\,c^2}{4}\dfrac{\partial B_z}{\partial x} \\ -\dfrac{c^2}{4}\dfrac{\partial B_z}{\partial x} \\ -c\dfrac{\partial E_y}{\partial x} \end{bmatrix} + \begin{bmatrix} \dfrac{3\,c^2}{4}\dfrac{\partial B_z}{\partial y} \\ \dfrac{\sqrt{3}\,c^2}{4}\dfrac{\partial B_z}{\partial y} \\ c\dfrac{\partial E_x}{\partial y} \end{bmatrix}.$$

3.1. Two-Dimensional Test Cases

To test the efficacy of the D4–RK4 scheme, a geometry involving a 2λ square cylinder with a TE_z pulse obliquely incident at an angle of $\phi = 45^\circ$ (with respect to the x-axis) is chosen. To properly handle the domain truncation, the GT-PML [15] is used with all D4–RK4 implementations. For the simulations described in this section a time derivative of a Gaussian pulse with parameters as described in Section 1.1 is used to model the incident fields. The time step in two dimensions is related to the special step size as $dt = (CFL\ h)/(\sqrt{2}v_p)$. All simulations are run with a CFL $= \sqrt{2}/2$ (i.e., the pulse propagates one cell along a Cartesian axis every two time steps).

Figure 7 shows the surface current data for both the D4–RK4 at 40 points per wavelength (ppw) and a Yee [16, 17] scheme of the same configuration at 80 ppw. The current data is obtained using a running Fourier transform on the input signal and total magnetic field at the surface of the scatterer. Figure 8 shows the phase of the surface current for both schemes. The classic Yee scheme has been used extensively to model electromagnetic scattering objects, and to track surface currents for PEC objects [18]. The convergence of the two separate techniques toward the same answer provides verification for results obtained from the D4–RK4 scheme.

It should be noted that the comparisons (between the D4–RK4 and Yee scheme) contained herein suffice only to show the efficacy of the D4–RK4 scheme, and that no claims concerning the efficiency of the D4–RK4 over the Yee scheme are being made. Furthermore, since the Yee scheme uses an uncolocated grid [17], the current data (which utilizes H_z in this case) for the Yee calculation is actually taken at locations at least half a cell length *off* the scatterer (and a little more at the corners). For this reason, a higher number of ppw is used for the Yee scheme in order to move the actual geometries, used in the comparison, closer together.

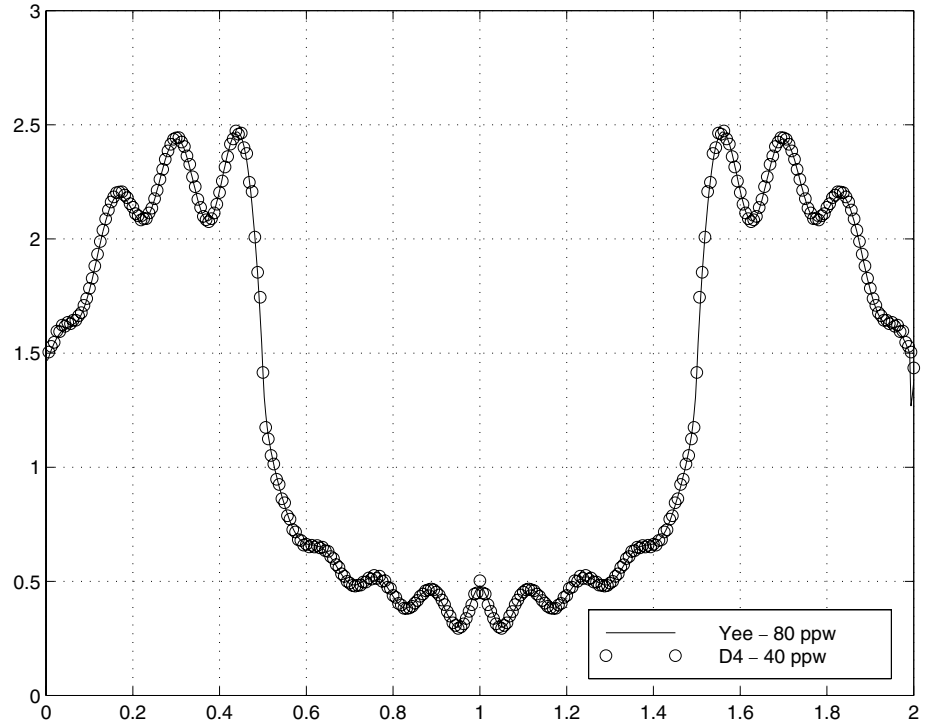

FIG. 7. Yee and D4 calculated surface currents for an obliquely incident TE_z wave on a 2λ square cylinder.

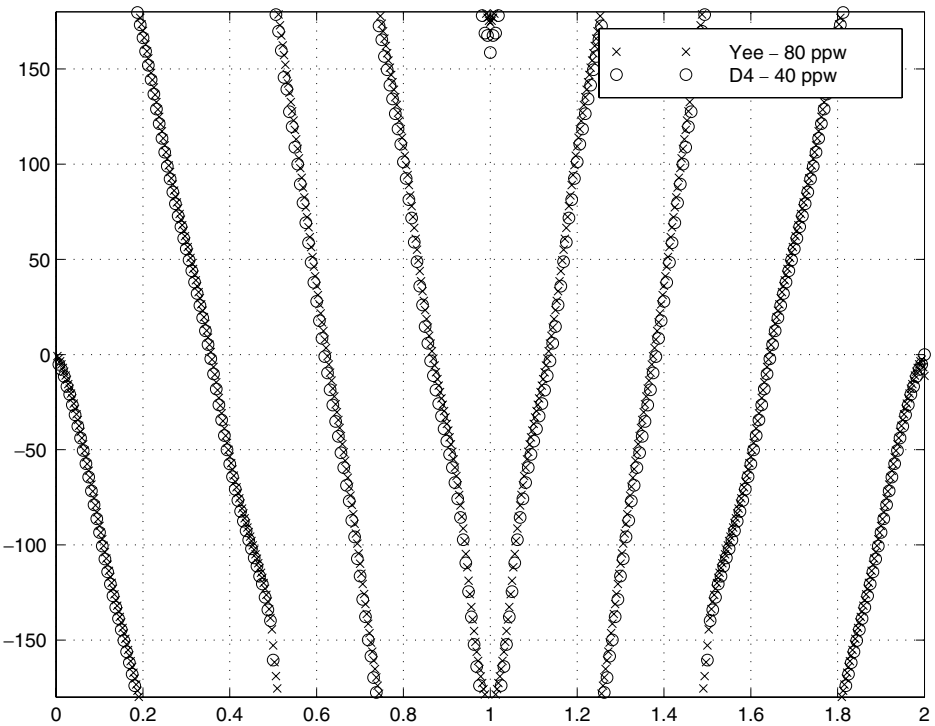

FIG. 8. Phase for current on 2λ square cylinder.

4. CONCLUSIONS

In this paper we studied the implementation of high-order boundary schemes for various hyperbolic system cases associated with the Maxwell equations in one dimension and two dimensions. Special attention was given to IBVPs which included PEC surfaces in the computational domain. A major underlying theme has been the importance of building time stability into the time-domain calculations, and to this end, we used derivative stencils which satisfy the summation-by-parts property to approximate the spatial derivatives, and the orthogonal projection method to introduce the boundary conditions.

Moreover, in the study of electromagnetics, it is well understood that the Maxwell equations, combined with the constitutive relations, can completely describe all macroscopic electromagnetic phenomena. The only items that separate one electromagnetic situation from another are the values of the electromagnetic parameters on/at the boundaries of the problem. Therefore it behooves us to know definitively which electromagnetic field components are tangential, and which components are normal at the boundary surfaces within our CEM simulations. In other words, without a definitive normal at every exterior surface point of objects within a colocated domain, the problem being computed is very ill posed. It has been found that for colocated Cartesian-based CEM schemes, if we do not make special considerations for what happens at edges and corners of scatterers in two or three dimensions, we run into a genuine surface-normal ambiguity problem. In this paper we have both identified and resolved the surface-normal ambiguity problem for two-dimensional geometries. (The discussion of colocated Cartesian-based three-dimensional geometries is the topic of a future paper.)

In summary, the primary contributions of this paper are the following.

1. It shows how to construct a suite of RK4-based high-order time-stable solvers in one dimension. The methodology employed shows that any restricted full norm or diagonal norm operator, which satisfies the summation-by-parts property, can effectively handle one-dimensional propagation in a time-stable manner.
2. It identifies and solves an outstanding problem inherent in all Cartesian-based colocated CEM methods. The author labeled this a surface-normal ambiguity problem. Utilizing the orthogonal projection method, which effectively chamfers any corners, we can now provide a definitive surface normal at all locations on the exterior surface of a scatterer.
3. It derives a method for producing high-order time-stable two-dimensional solvers for the Maxwell equations on a colocated grid. These two-dimensional solvers provide for a definitive surface normal at every exterior node of a scatterer, while also correctly evolving in time—in both a scattered field and a total field formulation—the field components at all locations in time-stable manner.

These results, enumerated above, have been supported by simulations and mathematical analysis as appropriate.

ACKNOWLEDGMENTS

The majority of this work was funded by the United States Department of Defense Experimental Program to Stimulate Competitive Research, Grant F49620-96-1-0469, administered by the Air Force Office of Scientific Research. This work was supported in part by a grant of HPC time from the DoD HPC Center on the NAVOCEANO DoD MSRC Cray T90.

REFERENCES

1. M. H. Carpenter, D. Gottlieb, and S. Abarbanel, Time-stable boundary conditions for finite-difference schemes solving hyperbolic systems: Methodology and application to high-order compact schemes, *J. Comput. Phys.* **111**, 220–236 (1994).
2. J. Shang, A perspective of computational electromagnetics in the time domain, AIAA Preprint 97–2356, *28th Plasmadynamics and Lasers Conference*, Atlanta, GA (1997).
3. P. Olsson, Summation by parts, projections, and stability. I, *Math. Comput.* **64**, 1035–1065 (1995).
4. P. Olsson, Summation by parts, projections, and stability. II, *Math. Comput.* **64**, 1473–1493 (1995).
5. B. Gustafsson, On the implementation of boundary conditions for the method of lines, Technical Report 195 (Dept. of Scientific Computing, Uppsala University, Uppsala, Sweden, April, 1997).
6. B. Strand, Summation by parts for finite difference approximations for d/dx, *J. Comput. Phys.* **110**, 47–67 (1994).
7. B. Strand, Numerical studies of hyperbolic IBVP with high-order finite difference operators satisfying a summation by parts rule, Technical Report 176 (Dept. of Scientific Computing, Uppsala University, Uppsala, Sweden, 1996).
8. B. Strand, Simulations of acoustic wave phenomena using high-order finite difference approximations, Technical Report 177 (Dept. of Scientific Computing, Uppsala University, Uppsala, Sweden, 1996).
9. M. H. Carpenter, D. Gottlieb, and S. Abarbanel, Stable and accurate boundary treatments for compact, high-order finite-difference schemes, *Appl. Numer. Math.* **12**, 55–87 (1993).
10. R. F. Harrington, *Time-Harmonic Electromagnetic Fields* (McGraw-Hill, New York, 1961).
11. S. Wolfram, *Mathematica* (Addison-Wesley, Reading, MA, 1993).
12. J. F. Nystrom and J. L. Young, k-space transfer function design of discrete operators: Application to maxwell's time domain equations, *J. Electromagn. Waves Appl.* **13**, 781–806 (1999).
13. H.-O. Kreiss and J. Lorenz, *Initial-Boundary Value Problems and the Navier-Stokes Equations* (Academic Press, San Diego, CA, 1989).
14. A. L. Fetter and J. D. Walecka, *Theoretical Mechanics of Particles and Continua* (McGraw-Hill, New York, 1980).
15. L. Zhao and A. C. Cangellaris, GT-PML: Generalized theory of perfectly matched layers and its application to the reflectionless truncation of finite-difference time-domain grids, *IEEE Trans. Microwave Theory and Tech.* **44**, 2555–2563 (1996).
16. K. S. Yee, Numerical solution of initial boundary value problems involving maxwell's equations in isotropic media, *IEEE Trans. Antennas Propag.* **14**, 302–307 (1966).
17. M. N. O. Sadiku, *Numerical Techniques in Electromagnetics* (CRC Press, Boca Raton, FL, 1992).
18. A. Taflove and K. R. Umashankar, Review of FD-TD numerical modeling of electromagnetic wave scattering and radar cross section, *Proc. IEEE.* **77**, 682–699 (1989).